Structural Characterization of Celgard® Microporous Membrane Precursors: Melt-Extruded Polyethylene Films

R. T. CHEN,[1,*] C. K. SAW,[1] M. G. JAMIESON,[1] T. R. AVERSA,[1] and R. W. CALLAHAN[2]

[1]Hoechst Celanese Research Division, Summit, New Jersey 07901; [2]Hoechst Celanese Separations Products Division, Charlotte, North Carolina 28273

SYNOPSIS

"Row nucleated lamellar" structures are formed when highly crystalline polymers are melt-extruded and recrystallized under high stress. Polyethylene (PE) and polypropylene (PP) films with row lamellar structures have been utilized to produce microporous membranes. Birefringence measurements of melt-extruded PE films show that improved film orientation can be achieved by annealing, extruding at higher speed, and using higher molecular weight polymers. Images from scanning tunneling, atomic force, and field emission scanning electron microscopy (STM, AFM, and FESEM) clearly show the lamellar structures in the melt-extruded PE and PP films. Microscopy results also show that surface lamellar textures are more pronounced with thicker lamellae and are better aligned along the extrusion direction after annealing. X-ray diffraction results show that the increase in film orientation can be attributed to increased lamellar perfection and orientation during annealing and also to better crystallite alignment along the machine direction with higher extrusion speed or with higher molecular weight. High-resolution capabilities of STM, AFM, and FESEM prove to be very effective tools in elucidating lamellar structures in polymeric membrane precursors and can be used as an aid in establishing structure–process–property relationships in making microporous membranes. © 1994 John Wiley & Sons, Inc.

INTRODUCTION

"Row nucleated lamellar" structures form when polymers capable of developing high crystallinity are melt-extruded and recrystallized under high stress.[1-7] This highly oriented lamellar morphology results in a unique class of materials—"hard elastic" polymers that exhibit unusually high elongation, high modulus, and high elastic recovery from high strains. This type of hard elastic behavior has been reported in polypropylene, polyoxymethylene copolymer (Celcon®, Hoechst Celanese), polyethylene, and 66 nylon when specially annealed.[4] Slitlike micropores can form in the melt-extruded films between the stacked lamellae after annealing and stretching in the machine (extrusion) direction. This process has been adopted to produce Celgard® microporous membranes (Hoechst Celanese) for separation applications.[8-10] To produce the desired pore morphology, row lamellar structures must be established in the membrane precursors, i.e., as-extruded and annealed polyethylene or polypropylene films or hollow fibers.

There has been extensive research on microstructures of "hard elastic" materials in the 1960s and early 1970s[1-7,11-14] using X-ray and microscopy techniques. Characteristics of "hard elastic" materials have been discussed in a review paper by Cannon et al.[5] Due to the lack of pronounced surface topography, the lamellar structures could not be directly examined by conventional microscopy. Lamellar structures in the "hard elastic" materials have typically been investigated by replica-TEM,[2,3,11,13] an indirect and time-consuming procedure. Recently, with the availability of high-resolution imaging techniques such as scanning tunneling microscopy (STM) and field emission scanning electron microscopy (FESEM), lamellar structures in the membrane precursors have been directly resolved for the first time.[15] Very little work has been

* To whom correspondence should be addressed.

Journal of Applied Polymer Science, Vol. 53, 471–483 (1994)
 CCC 0021-8995/94/050471-13

Table I Sample Summary and Birefringence Data

ID	Sample	Extrusion Rate	Treatment	Birefringence
A	PE[a]	Low	As-extruded	0.0132
B	PE[a]	Low	Annealed	0.0175
C	PE[a]	High	As-extruded	0.0213
D	PE[a]	High	Annealed	0.0282
E	PE[b]	Medium	As-extruded	0.0292
F	PE[b]	Medium	Annealed	0.0376
G	PP	High	Annealed	0.0216

[a] Lower molecular weight PE.
[b] Higher molecular weight PE.

done in the characterization of hard elastic materials since the early 1970s. Because of the availability of emerging high-resolution imaging techniques, there is a revived interest in examining lamellar morphologies in the Celgard® microporous membrane precursors. This study was initiated to demonstrate that the lamellar morphology can be monitored at the crucial precursor stage utilizing new techniques prior to pore formation (after stretching) and to develop a better understanding of the structure–process–property relationships in making microporous membranes.

The degree of orientation in the polyethylene (PE) and polypropylene (PP) melt-extruded films is a critical parameter in making controlled pore structures in the Celgard® membranes. The film orientation is typically characterized by birefringence, which can be attributed to lamellar orientation and to molecular orientation. In addition to a comprehensive microscopy study (FESEM, STM, and AFM) of the lamellar morphology, complementary techniques such as wide-angle X-ray scattering (WAXS) and small-angle X-ray scattering (SAXS) were carried out to determine the contributions of film orientation from molecular orientation, crystallite sizes, lamellar spacing, and order.

EXPERIMENTAL

Materials

The materials investigated include polyethylene (PE) and polypropylene (PP) flat-sheet membranes (Celgard®, trade mark of Hoechst Celanese Corp.) and their precursors. Low and high molecular weight PE precursor films (ca. 25 μm thick) made with different extrusion speeds, both as-extruded and annealed, as well as a PP Celgard® precursor film were selected for this study (see sample summary in Table I).

Birefringence Measurements (Optical Microscopy)

The birefringence of the film samples were measured on a Leitz polarizing microscope using Berek tilt-type compensators with varying orders of retardation.

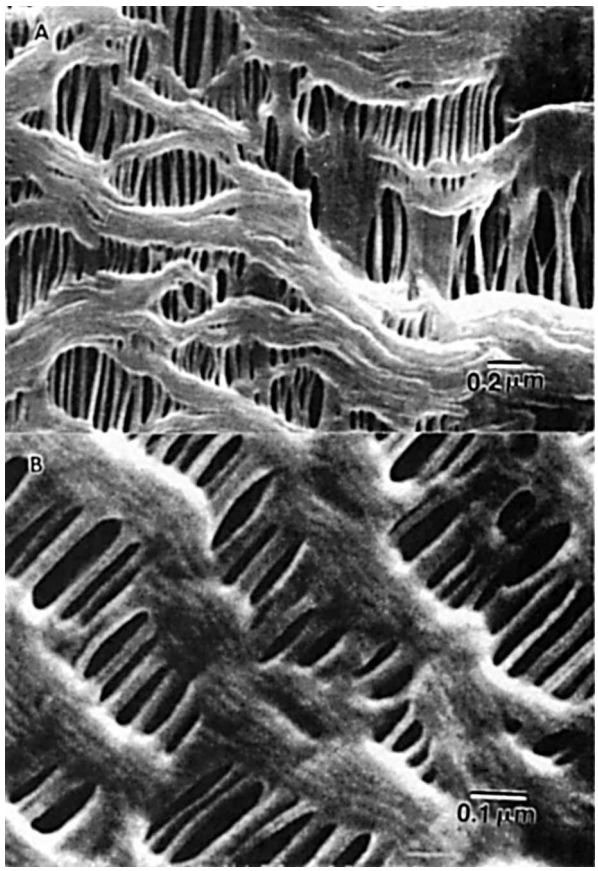

Figure 1 FESEM images showing micropores in Celgard® microporous membranes: (a) PE; (b) PP.

Field Emission Scanning Electron Microscopy (FESEM)

The samples were coated with ca. 2 nm Pt using ion-beam sputtering with argon gas (Ion Tech., Ltd.). FESEM imaging was conducted on a JEOL 840F field emission SEM operating at 5 kV. Electron-beam damage was found to be significantly reduced at this low voltage.

Scanning Tunneling Microscopy (STM)

The film samples were mounted on silicon substrates and then coated with ca. 5 nm Pt using an ion-beam sputtering (IBS) unit. The 5 nm Pt coating prepared by IBS has been previously shown to introduce minimal topography to the original surfaces.[16] STM imaging was performed on a Nanoscope III STM (Digital Instruments) using a bias voltage of 100 mV and a tunneling current of 1 nA.

Atomic Force Microscopy (AFM)

AFM imaging was performed on a Nanoscope III contact-type AFM (by Digital Instruments, Santa Barbara, CA) using a long-range scanner (84 μm max. scan range). A microfabricated cantilever (200 μm long) with a pyramidal Si_3N_4 tip was used to scan the surface and the cantilever deflections (force) were monitored using a laser beam and a position sensitive photodetector. An optical microscope attachment was used for tip alignment and for guiding the AFM tip to the areas of interest. The imaging was operated using a constant force mode with a repulsive force of ca. 10^{-9} Newtons.

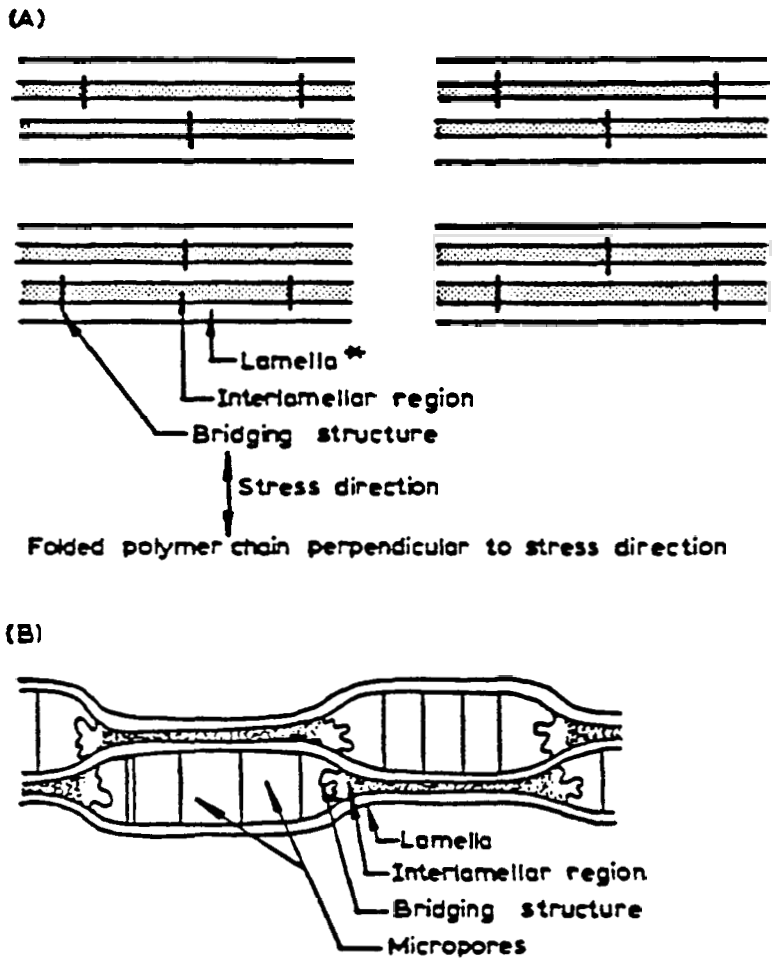

Figure 2 Schematic of row nucleated lamellae in (a) Celgard® precursor and (b) microporous Celgard film (after stretching). Reprinted with permission from H. S. Bierebaum, R. B. Isaacson, M. L. Druin, and S. G. Plovan, *Ind. Eng. Chem. Prod. Res. Dev.*, **13**, 2 (1974), copyright 1974 American Chemical Society.

Wide/Small Angle X-ray Scattering (WAXS/SAXS)

The WAXS patterns were acquired using the conventional flat-plate technique. Monochromatized copper Kα radiation was utilized. The digitized spectra was used to determine the orientation function, peak positions, and the degree of crystallinity were acquired using a specially modified Philips vertical goniometer with the ability to rotate the film in the direction perpendicular to the scattering plane. Essentially, this technique provides two-dimensional mapping of the diffraction pattern and maintains the θ–2θ coupling (Bragg condition). The X-ray beam is incident onto the sample in the direction perpendicular to the film surface.

The degree of crystallinity is estimated by calculating the area of the crystalline peaks at different azimuthal angles (weighted by the cosine of the angle) to the total scattering area. The crystallite size is determined by the full-width at half-maximum of the (110) reflection with an instrumental correction.

The SAXS experiments were carried out on a Rigaku pinhole small-angle apparatus mounted on a high-intensity rotating anode generator. Filtered CuKα radiation was used for the experiment and a microdensitometer was used to calculate the lamellar spacings.

RESULTS AND DISCUSSION

Birefringence Results

The degree of orientation in the PE and PP melt-extruded precursor films is a critical parameter in developing controlled pore structures in the membranes. Birefringence measurements using optical microscopy is a most effective way of characterizing the gross orientation of the Celgard® membrane

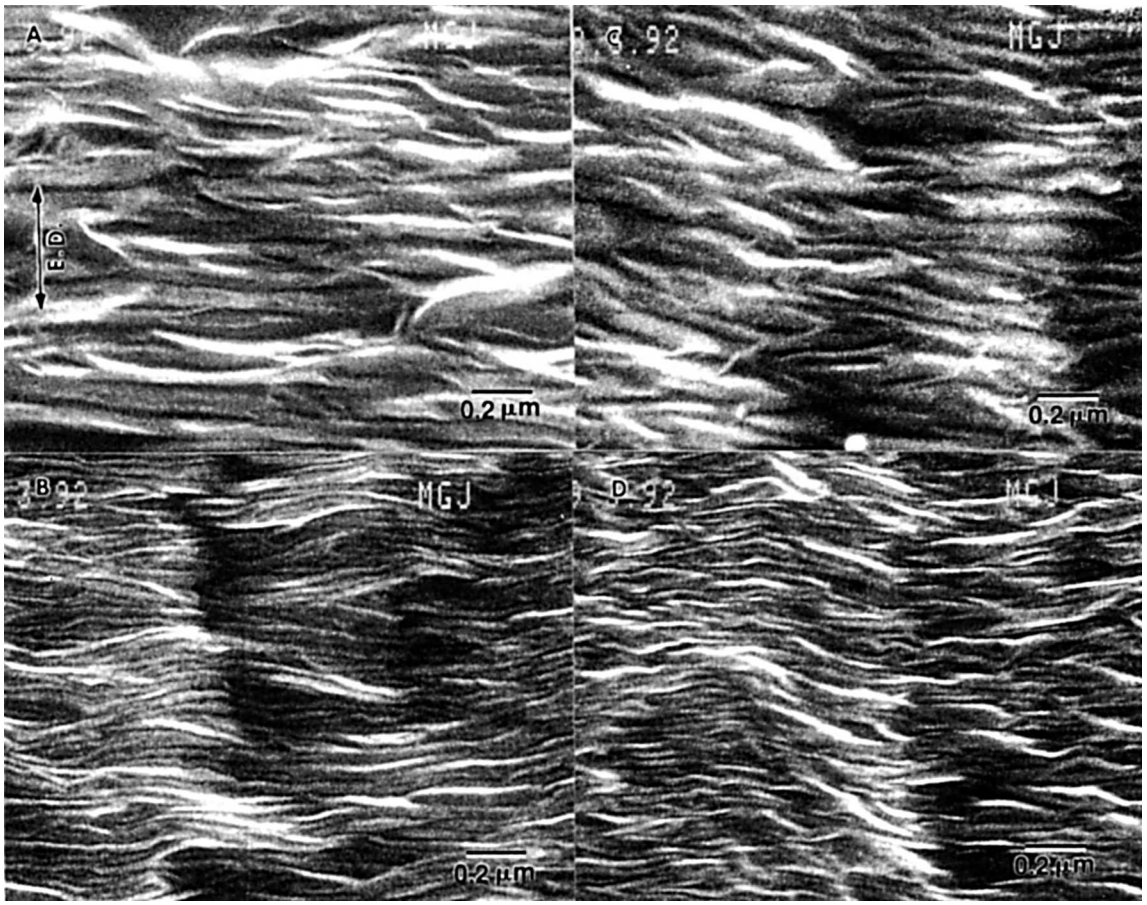

Figure 3 FESEM images of low molecular weight PE precursor films: (a) low extrusion rate (E.R.), as-extruded; (b) low E.R., annealed; (c) high E.R., as-extruded; (d) high E.R., annealed (E.D. is the extrusion direction).

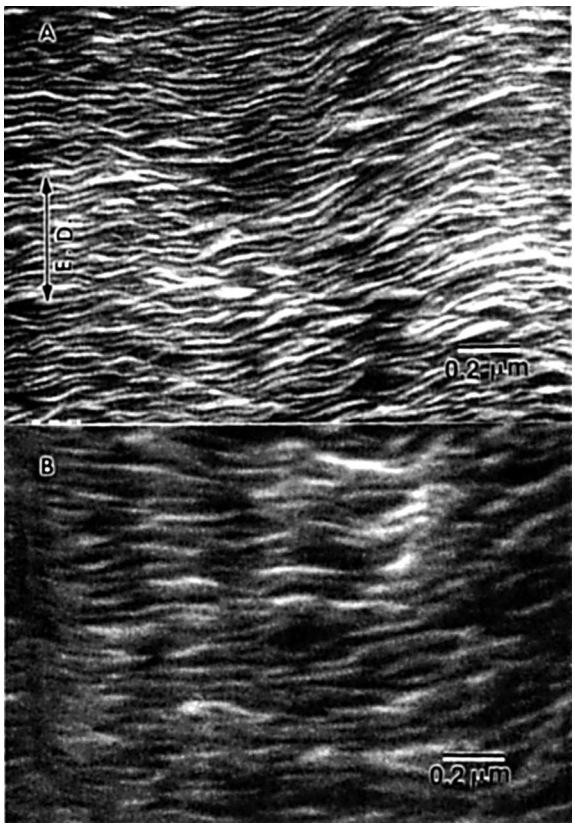

Figure 4 FESEM images of high molecular weight PE precursor films: (a) as-extruded; (b) annealed (E.D. is the extrusion direction).

precursors. As shown in the birefringence data in Table I, gross orientation in the PE film precursors increases with extrusion rate and molecular weight. Annealing at high temperature was also found to be very effective in increasing the overall film orientation. As film orientation (birefringence) can be attributed to lamellar orientation and to molecular orientation, microscopy and X-ray scattering experiments were also carried out to determine the origin of birefringence increase.

FESEM Results

The membranes exhibit slitlike micropores typically ca. 0.05 and 0.02 μm long for PE and PP Celgard® membranes, respectively (Fig. 1). The slitlike micropores are organized in a pocket fashion, a direct result of stretching row nucleated lamellae stacks. In some cases, traces of lamellae and bridging fibrils between slitlike pores are also evident in the FESEM micrographs. Microporous structures in Celgard and the mechanism of slitlike pore formation has previously been extensively studied.[8,10] A schematic showing row nucleated lamellae in the precursor films and micropores in the Celgard® membranes is included in Figure 2.[8] It is noted that a smoother surface with better organized slit-pores in the pore pockets is present in the PP Celgard® than in PE Celgard® membranes. These differences in pore morphology, which are closely related to the differences in lamellar organization in the precursor films, were illustrated by STM imaging.

FESEM images of the low molecular weight PE films with different extrusion rates and thermal histories are shown in Figure 3. The FESEM images clearly show bundles (stacks) of lamellae in the as-extruded film and individual lamellae (edge-on view) in the annealed PE precursors. Upon annealing, the lamellae thicken and tilt toward better alignment with respect to the normal of the film plane. In this way, the individual lamella exhibits more pronounced topography and thereby makes FESEM imaging of individual lamella possible. The FESEM images also show that the lamellae are better aligned with respect to the machine (extrusion) direction in the annealed PE film than in the as-extruded sample. Finer lamellar structures with slight reduction in lamellar thickness were also found in the PE film precursors made at a high extrusion rate. FESEM images of the high molecular weight (M.W.) PE films are shown in Figure 4, in which individual lamella morphology can be resolved in the as-extruded films because of the increase in thickness and alignment of the lamellae. This type of lamellar morphology is very similar to the annealed PE precursor with lower molecular weight.

STM/AFM Results

Both STM of Pt-coated samples and AFM of uncoated films were performed to explore the lamellar textures in the Celgard® precursors. As most of the lamellae have thicknesses greater than 10 nm, no significant differences will result from these two different techniques. STM images of the low molecular weight PE films are shown in Figure 5 and AFM images of the high molecular weight PE films are shown in Figure 6. In the black-and-white STM/AFM images shown (e.g., Fig. 6), the heights of the surface topography were gray-level coded, with darker areas representing lower points on the sample surfaces. As shown in Figure 5(a) and (c), individual fine lamellae ca. 10–30 nm thick can be resolved in the as-extruded PE films, whereas FESEM imaging reveals only lamellar stacks [Fig. 3(a) and (c)]. The FESEM, STM and AFM images of the PE pre-

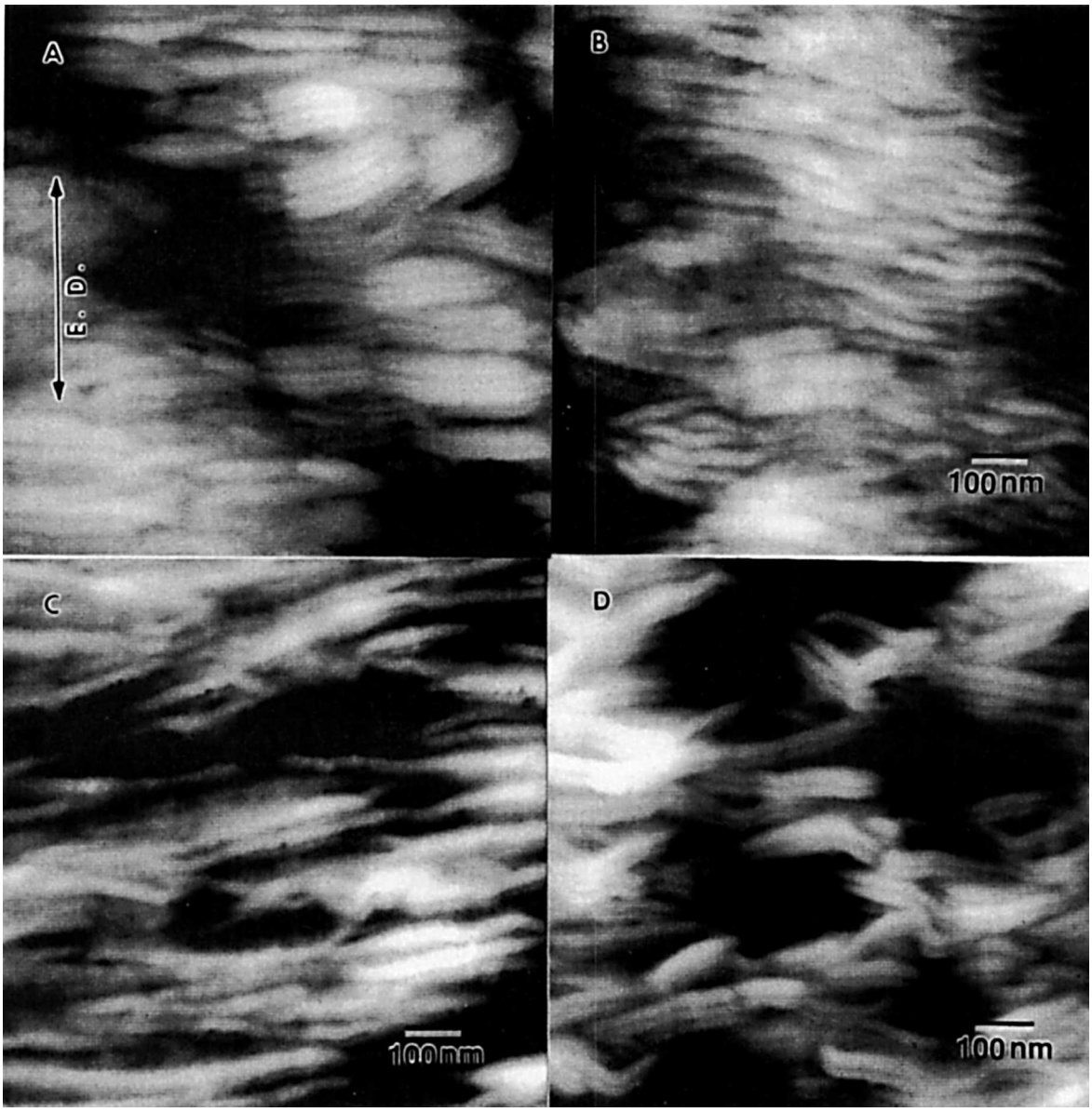

Figure 5 STM images of PE precursor film: (a) low E.R., as-extruded; (b) low E.R., annealed; (c) high E.R., as-extruded; (d) high E.R., annealed (E.D. is the extrusion direction).

cursors show that surface lamellar textures are more pronounced and more aligned with respect to the extrusion direction in the annealed films than in the as-extruded films. The meandering nature of the lamellae is also evident in the STM/AFM images. Since the STM/AFM images were acquired in digitized format, lamellar spacing (or thickness) can be readily obtained by either directly measuring individual lamella or using one-dimensional Fourier transform to extract periodicity. Using these techniques, average lamellar thicknesses were measured from typical STM/AFM images for each sample and the results are summarized in Table II. Lamellar thickening was evident from the STM data. The STM results also show good agreement with the SAXS results, although it is recognized that STM/AFM is a direct microscopic method for individual lamella on the surface, whereas SAXS is a macroscopic technique for extracting average lamellar spacing in the bulk of the film.

For comparison, an STM image of an annealed PP Celgard® precursor film is also included in Figure

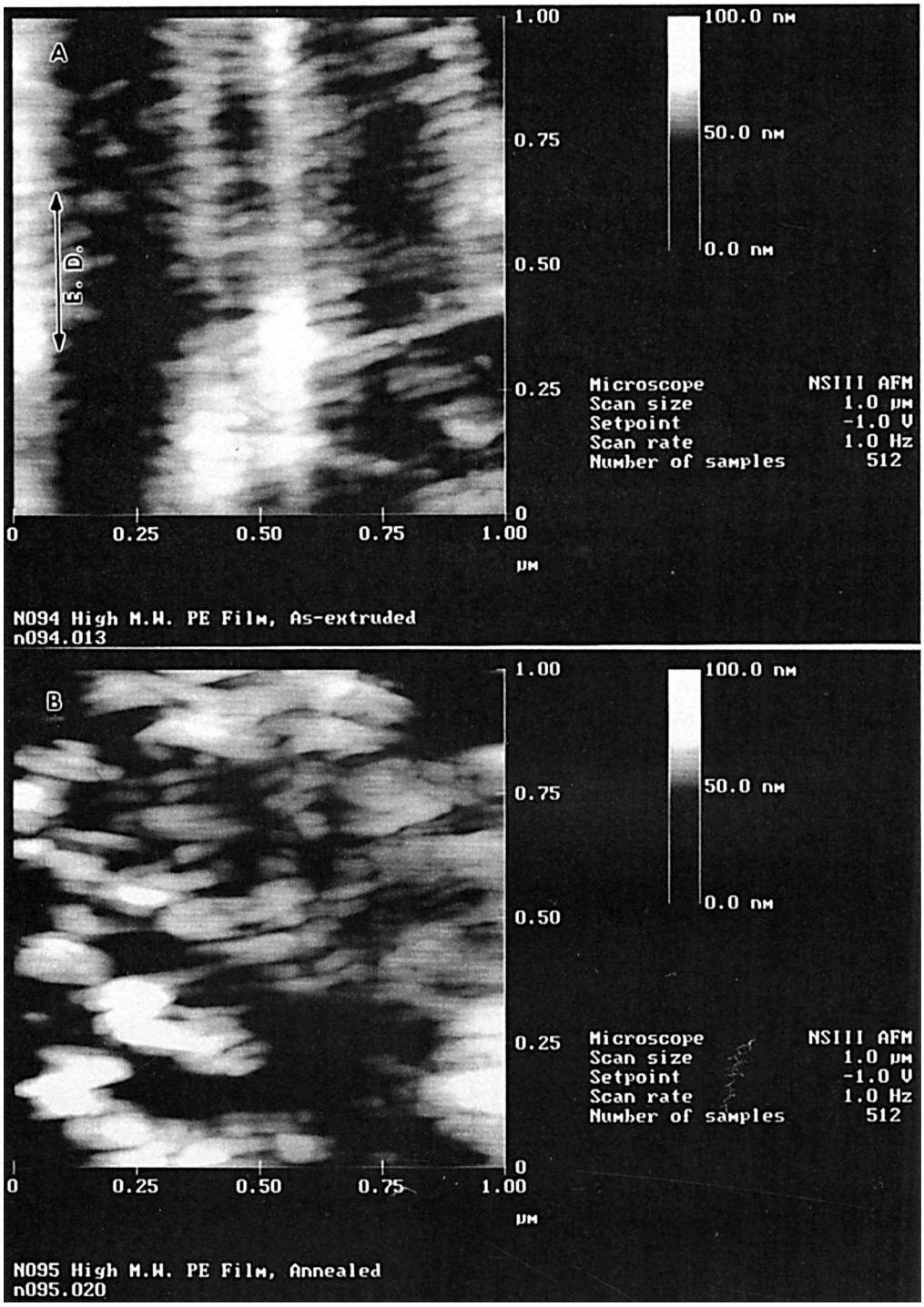

Figure 6 AFM images of high molecular weight PE precursor films: (a) as-extruded; (b) annealed (E.D. is the extrusion direction).

7, which shows that the lamellae in the PP precursor films have very little topography and are very difficult to resolve even by high-resolution FESEM. By STM imaging, the lamellar structures in the PP film precursors are found to be less pronounced and less extended than in the PE film precursors. This difference in lamellar structures in the film precursors results in different surface pore morphologies between the PE and PP Celgard® membranes (Fig. 1), i.e., PP Celgard® membranes exhibit less three-

Table II Measurements of Lamellar Spacing in PE Films

	Sample					
	A	B	C	D	E	F
Birefringence	0.0132	0.0175	0.0213	0.0282	0.0292	0.0376
Mean lamellar spacing (Å) (by STM/AFM)	198	268	242	309	263	311
Mean lamellar spacing (Å) (by SAXS)	239	274	247	278	247	282

dimensional topography (interpore fibrils are more at the same height level) and more uniform porous structures with smaller pores than the PE membranes.

WAXS/SAXS Results

Typical WAXS diffraction patterns from the as-extruded and annealed PE film precursors are included in Figure 8. The vertical direction corresponds to the machine direction of the film. The patterns indicate the presence of an orthorhombic PE structure (with a = 7.40 Å, b = 4.94 Å, and c = 2.54 Å [Ref. 17]) with (110) being the strongest reflection. There are four possible (110) and (020) reflections, and these peaks may overlap depending on the crystallite alignment. Since the (020) peak is better defined, the (020) reflection is used to determine the molecular orientation function.[18]

The alignment of the crystallites with respect to the extrusion axis can be monitored by the tilt angle ($\Delta\Phi$), determined from the angle between the (110) reflection and the horizontal axis. The changes in the tilt angle represent the alignment of the molecular chains with respect to the extrusion direction. A small tilt angle ($\Delta\Phi$) represents better alignment of the crystallites with respect to the extrusion direction. It has been shown that this tilt angle

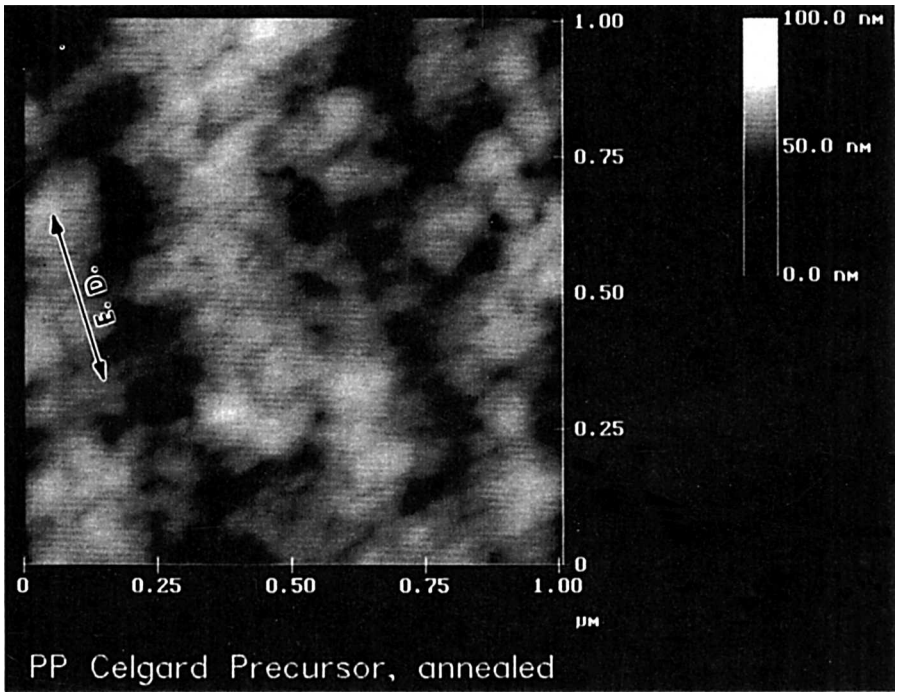

Figure 7 STM image showing typical lamellar morphology in an annealed PP Celgard precursor film (E.D. is the extrusion direction).

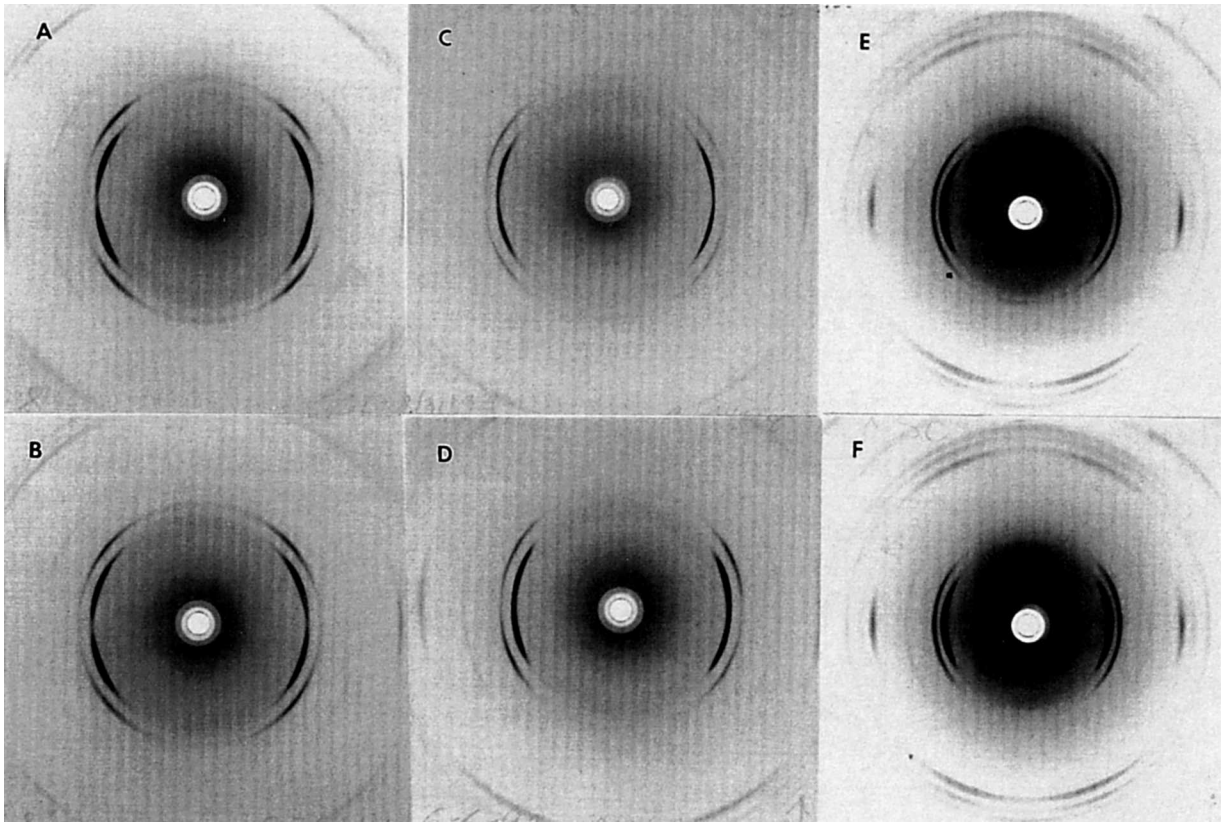

Figure 8 WAXS patterns of PE Celgard® precursor films: (a) low E.R., as-extruded; (b) low E.R., annealed; (c) high E.R., as-extruded; (d) high E.R., annealed; (e) high M.W., as-extruded; (f) high M.W., annealed.

changes with different spinning conditions for fibers.[19] Similar effects of extrusion conditions are expected in the highly oriented melt-extruded films.

The results extracted from the WAXS patterns are summarized in Table III. Only a slight increase in overall crystallinity can be observed with annealing. The orientation factor also remains very high and similar in all cases. The (110) d-spacings of the crystalline reflections do not change significantly between these samples whether they are an-

Table III WAXS Results on PE Celgard® Precursors

	Sample					
	A	B	C	D	E	F
Birefringence	0.0132	0.0175	0.0213	0.0282	0.0292	0.0376
d-Spacing (Å) (110)	4.11	4.12	4.12	4.11	4.11	4.11
Crystallite size (Å)	88	88	88	87	99	101
Crystallinity	65%	64%	66%	70%	61%	66%
$\Delta\phi$ (110)[a]	21.3°	21.2°	16.9°	14.8°	~ 10°	~ 7°
f_c (020)[b]	0.967	0.962	0.960	0.951	0.950	0.946

[a] $\Delta\phi$ (110) is a measure of crystallite alignment with respect to machine direction.
[b] f_c: Herman orientation factor, describing the distribution of crystal alignment.

Table IV SAXS Results on PE Celgard® Precursors

	Sample					
	A	B	C	D	E	F
Birefringence	0.0132	0.0175	0.0213	0.0282	0.0292	0.0376
Mean lamellar spacing (Å)	239	274	247	278	247	282
Δ^a (cm)	0.80	0.58	0.65	0.50	0.73	0.55

[a] Δ is a measure of distribution of lamellar spacings (or widths).

nealed or not, suggesting that the crystal structure is unaltered. Also, the crystallite sizes extracted do not show significant increases with annealing. However, the high molecular weight PE samples appear to show a small increase in crystallite size after annealing. Nevertheless, the decrease in the tilt angle can be observed in the samples with increasing birefringence. The effects of extrusion speed and molecular weight on the crystallite alignment are further illustrated in the azimuthal plot of (110) reflections in Figure 9. These results suggest that better alignment of the crystallites in the extrusion

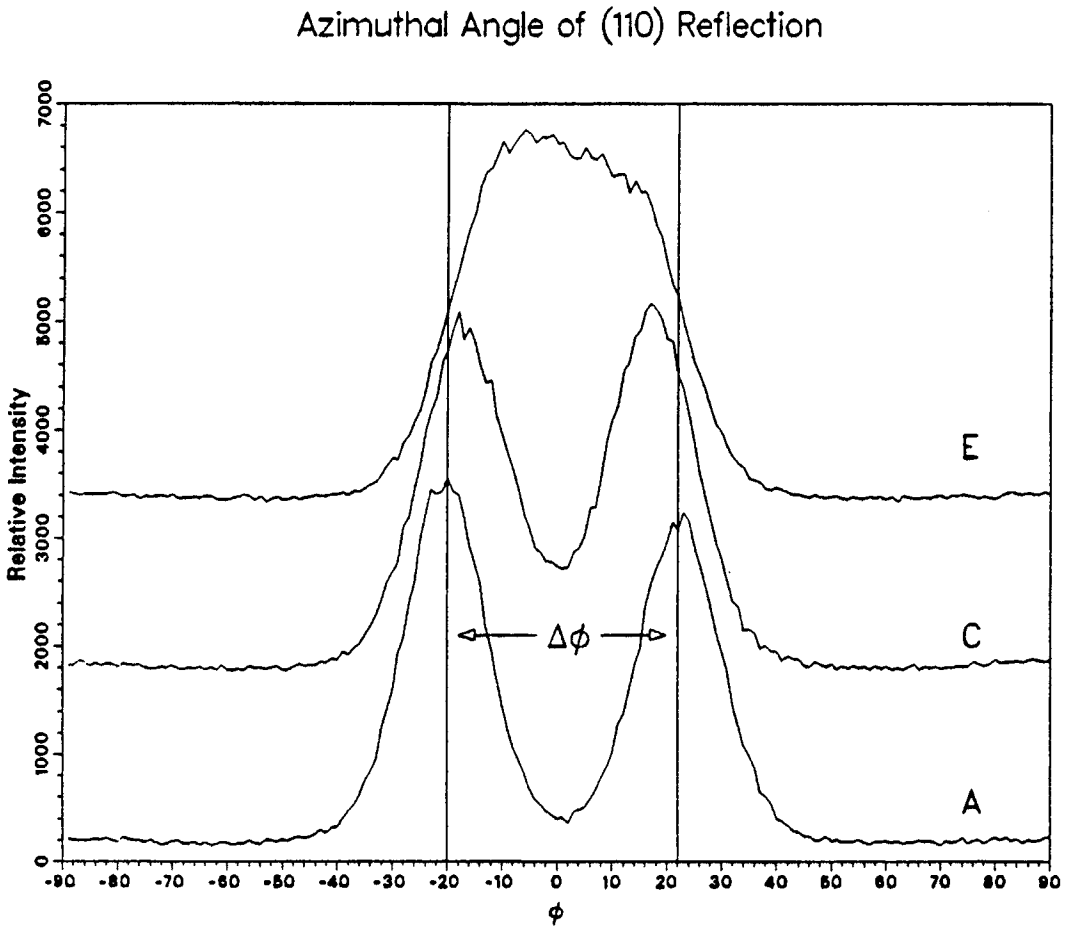

Figure 9 Plot of X-ray intensity vs. azimuthal angle of (110) reflection of as-extruded PE precursor films, Sample A: low M.W., low extrusion rate; sample C: low M.W., high extrusion rate; sample E: high M.W., medium extrusion rate.

direction is present after annealing, which can occur through either tilting of individual crystals or tilting of lamellae toward the extrusion axis.

Typical results of the SAXS experiments are shown in Figure 10 for the as-extruded and annealed PE film samples. SAXS pattern of the oriented PE film consists of two spots, one above and one below the origin. By measuring the positions of these peaks, the lamellar spacing can be calculated. The results of these calculations are listed in Table II. The spread of these peaks are also measured to determine the statistical distribution of the lamellar spacings (see Table IV). A reduction in the spread indicates an improvement of the distribution order. The results show that the samples with higher birefringence typically have higher lamellar spacing. Upon annealing, increase in lamellar spacing as well as improvement in the uniformity of lamellar spacing are observed.

General Discussion

Birefringence measurements provide an efficient tool for quickly assessing gross film orientation that can be attributed to molecular alignment as well as lamellar thickness and lamellar orientation. The birefringence results show that annealing, higher extrusion speeds, and higher molecular weight promote film orientation. STM/AFM, FESEM imaging, and SAXS/WAXS were conducted to determine the factors affecting higher film orientation. Because of their superior resolution (better than 0.1 nm in height), STM/AFM were capable of resolving individual fine lamellae even in the as-extruded PE and PP precursor films that were difficult to resolve by FESEM. For the low molecular weight PE films, the slight increase in the lamellar thickness and better alignment with respect to the plane normal of the film make lamellar structures on the surfaces more distinct and made FESEM imaging individual lamella in the annealed films possible.

In addition to a slight increase in crystallinity with annealing, wide-angle X-ray results show that basic crystal lattice structure, crystallite size, and orientation factors do not vary significantly with different extrusion speeds or annealing conditions. A significant decrease in the tilt angle defined by the (110) reflection and the horizontal axis in the WAXS pattern was observed in the films at higher extrusion speeds. It was therefore concluded that

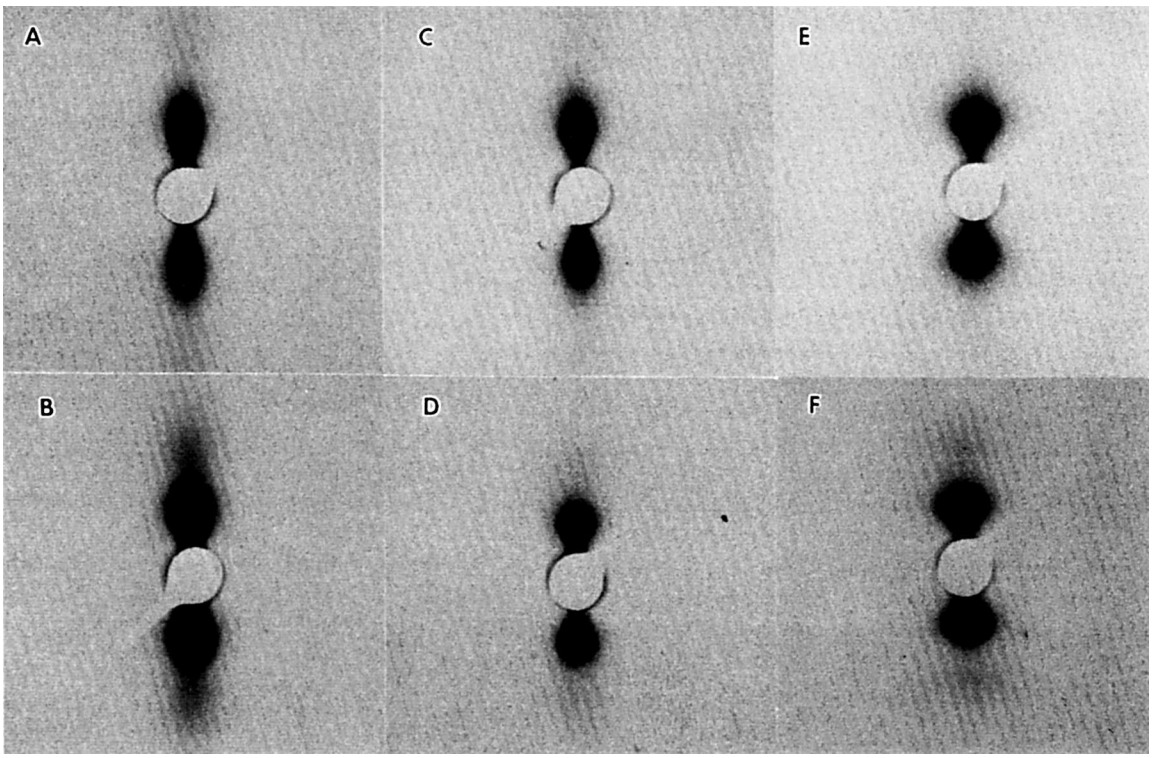

Figure 10 SAXS patterns of PE Celgard® precursor films: (a) low E.R., as-extruded; (b) low E.R., annealed; (c) high E.R., as-extruded; (d) high E.R., annealed; (e) high M.W., as-extruded; (f) high M.W., annealed.

better crystallite alignment with respect to extrusion direction may contribute to higher orientation in the film. It could occur either through tilting of the individual crystallite or through collective movement by lamellar tilting. In agreement with microscopy observations, small-angle X-ray results also show that annealing increases lamellar spacing as well as uniformity of the lamellar spacings.

In summary, STM/AFM and FESEM images show the lamellar structures in Celgard film precursors and that surface lamellar textures are more pronounced and more aligned with respect to the machine direction and to the film plane normal. Small-angle X-ray results show a slight increase in lamellar spacing (or widths) in the annealed film compared to the as-extruded film and show high lamellar spacing in both high molecular weight PE films. Wide-angle X-ray results indicate that higher extrusion rate results in better crystallite alignment along the machine direction. Based on these data, it can be concluded that the increase in film orientation can be attributed to increased lamellar thickness and perfection by annealing and can be attributed to increased crystallite alignment with the machine direction at higher extrusion speed. This study also demonstrates that high-resolution capabilities of STM/AFM and FESEM can provide unique opportunities for elucidating lamellar structures in polymers and in gaining insight about the nucleating fibrils for row lamellae and tie fibrils between lamellar stacks.

CONCLUSIONS

In combination with the conventional X-ray scattering techniques, high-resolution imaging such as FESEM and STM/AFM provide new tools for elucidating lamellar structures in polymers. The results of our investigation on the melt-extruded PE and PP films are summarized as follows:

1. The degree of orientation in the PE and PP melt-extruded films is a critical parameter in making controlled pore structures in the membranes. The birefringence measurements using optical microscopy show that both annealing and higher extrusion speed promote film orientation.
2. STM/AFM and FESEM images clearly show the lamellar structures in PE precursors. The surface lamellar textures are found to be more pronounced and more aligned with respect to the machine direction and to the film plane normal in the annealed films than in the as-extruded films.
3. SAXS results show increase in lamellar spacing as well as improvement in the distribution order of lamellar spacing upon annealing. WAXS results indicate that annealing results in a slight increase in crystallinity and that a higher extrusion rate results in better crystallite alignment with respect to the extrusion direction.
4. The increase in film orientation can be attributed to increased lamellar perfection and orientation during annealing and to better crystallite alignment along the extrusion direction with a higher extrusion speed. Higher molecular weight is also found to increase film orientation and lamellar thickness.
5. Lamellar structures in the PP film precursors are less pronounced and less extended than in the PE counterparts. This difference in lamellar structures in the film precursors does result in a different surface pore morphology in the PP membranes, which exhibit less three-dimensional and more uniform porous structures than do the PE membranes.
6. Complementary STM/AFM, FESEM, and WAXS/SAXS techniques provide insights for developing structure–property–process relationships in making microporous membranes.

The authors would like to acknowledge K. V. Nguyen for the optical birefringence measurements and K. A. Steele for sample preparation. Valuable suggestions by F. Haimbach and D. G. Vickroy at the Hoechst Celanese Research Division are also gratefully appreciated.

REFERENCES

1. A. Keller and M. J. Marchin, *J. Macromol. Sci.*, **B1**, 41 (1967).
2. C. A. Garber and E. S. Clark, *J. Macromol. Sci. Phys.*, **B4**(3), 499 (1970).
3. K. Neki and P. H. Geil, *J. Macromol. Sci. Phys.*, **B9**(1), 71 (1974).
4. B. S. Sprague, *J. Macromol. Sci. Phys.*, **B8**, 157 (1973).
5. S. L. Cannon, G. B. McKenna, and W. O. Statton, *J. Polym. Sci. Macromol. Rev.*, **11**, 209 (1976).
6. R. G. Quynn and H. Brody, *J. Macromol. Sci. Phys.*, **B4**(4), 953 (1970).
7. R. G. Quynn and H. Brody, *J. Macromol. Sci. Phys.*, **B5**(4), 721 (1971).
8. H. S. Bierenbaum, R. B. Isaacson, M. L. Druin, and

S. G. Plovan, *Ind. Eng. Chem. Prod. Res. Dev.*, **13**, 2 (1974).
9. R. Callahan, *AICHE Symp.*, **84**(261), 54 (1988).
10. T. Sarada, L. C. Sawyer, and M. I. Ostler, *J. Membr. Sci.*, **15**(1), 97 (1983).
11. K. Sakaoku and A. Peterlin, *J. Macromol. Sci.*, **B1**, 103 (1967).
12. A. Peterlin and K. Sakaoku, *Kolloid Z.*, **212**, 51 (1966).
13. P. Y.-F. Fung and S. H. Carr, *J. Macromol. Sci. Phys.*, **B6**(4), 621 (1972).
14. H. D. Noether and W. Whitney, *Kolloid Z. Z. Polym.*, **251**, 991 (1973).
15. R. T. Chen, M. G. Jamieson, and R. Callahan, in *Proceedings of the 50th Annual Meeting of the EMSA*, San Francisco Press, San Francisco, 1992.
16. I. H. Musselman and P. E. Russell, *Microbeam Analysis—1989*, P. E. Russell, Ed., San Francisco Press, San Francisco, CA, 1989, p. 535.
17. C. W. Bunn and T. C. Alcock, *Trans. Faraday Soc.*, **41**, 317 (1945).
18. L. E. Alexander, *X-ray Diffraction Methods in Polymer Science*, Wiley-Interscience, New York, 1969.
19. K. Katayama, T. Amano, and K. Nakamura, *Kolloid Z. Z. Polym.*, **226**, 125 (1968).

Received August 11, 1993
Accepted November 11, 1993